Autotaxin Secretion Is a Stromal Mechanism of Adaptive Resistance to TGFβ Inhibition in Pancreatic Ductal Adenocarcinoma

Silvia Pietrobono[1], Fabio Sabbadini[1], Monica Bertolini[1], Domenico Mangiameli[1], Veronica De Vita[1], Federica Fazzini[2], Giulia Lunardi[1], Simona Casalino[1], Enza Scarlato[1], Valeria Merz[1], Camilla Zecchetto[1], Alberto Quinzii[1], Giusy Di Conza[3], Michael Lahn[3], and Davide Melisi[1,2]

ABSTRACT

The TGFβ receptor inhibitor galunisertib demonstrated efficacy in patients with pancreatic ductal adenocarcinoma (PDAC) in the randomized phase II H9H-MC-JBAJ study, which compared galunisertib plus the chemotherapeutic agent gemcitabine with gemcitabine alone. However, additional stromal paracrine signals might confer adaptive resistance that limits the efficacy of this therapeutic strategy. Here, we found that autotaxin, a secreted enzyme that promotes inflammation and fibrosis by generating lysophosphatidic acid (LPA), mediates adaptive resistance to TGFβ receptor inhibition. Blocking TGFβ signaling prompted the skewing of cancer-associated fibroblasts (CAF) toward an inflammatory (iCAF) phenotype. iCAFs were responsible for a significant secretion of autotaxin. Paracrine autotaxin increased LPA-NFκB signaling in tumor cells that triggered treatment resistance. The autotaxin inhibitor IOA-289 suppressed NFκB activation in PDAC cells and overcame resistance to galunisertib and gemcitabine. In immunocompetent orthotopic murine models, IOA-289 synergized with galunisertib in restoring sensitivity to gemcitabine. Most importantly, treatment with galunisertib significantly increased plasma levels of autotaxin in patients enrolled in the H9H-MC-JBAJ study, and median progression-free survival was significantly longer in patients without an increase of autotaxin upon treatment with galunisertib compared with those with increased autotaxin. These results establish that autotaxin secretion by CAFs is increased by TGFβ inhibition and that circulating autotaxin levels predict response to the combination treatment approach of gemcitabine plus galunisertib.

Significance: TGFβ inhibition skews cancer-associated fibroblasts toward an inflammatory phenotype that secretes autotaxin to drive adaptive resistance in PDAC, revealing autotaxin as a therapeutic target and biomarker of galunisertib response.

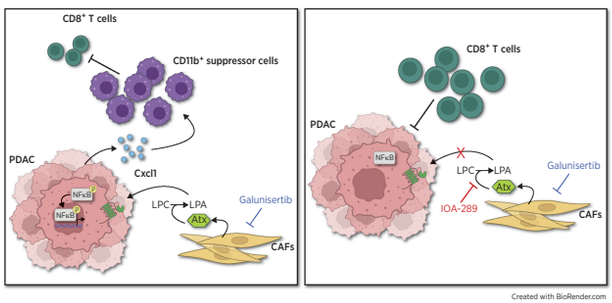

Introduction

Pancreatic ductal adenocarcinoma (PDAC) remains the most lethal and poorly understood human malignancy (1). Considering all stages combined, PDAC still has the lowest 5-year relative survival rate among solid tumors at 12% (2) and is projected to become the second leading cause of cancer-related death by 2040 in Western countries (3). The poor prognosis for patients affected by PDAC is mainly attributed to the early metastatic behavior, its aggressive course, and the limited efficacy of currently approved chemotherapeutic treatments (4).

The TGFβ is the most recurrently mutated signal transduction pathway in PDAC (5). TGFβ maintains homeostasis in normal tissues. However, being genetically unstable, cancer cells have the capacity to circumvent this suppressive function and render TGFβ signaling to promote tumor growth, epithelial-to-mesenchymal transition, and metastasis (6, 7). Under these conditions, TGFβ signaling plays a key role in remodeling the tumor stromal microenvironment by reprogramming the cancer-associated fibroblasts, or CAFs (8). In PDAC specifically, TGFβ and IL1 are secreted by tumor cells and counteract each other to balance the skewing of CAFs toward a myofibroblastic (myCAF) or an inflammatory (iCAF) phenotype, respectively (9).

In the recent years, we have contributed to demonstrate that inhibition of the TGFβ signaling is a potential strategy for the treatment of patients affected by PDAC. We initially showed the therapeutic efficacy of pharmacologic inhibition of both Smad-dependent and Smad-independent pathways in reverting the intrinsic chemoresistance of this disease in preclinical models (10, 11). These results led us to investigate clinically the inhibition of TGFβ signaling in combination with chemotherapeutic (12–14) or immunotherapeutic agents (15) as a novel treatment strategy for patients with PDAC. In an initial phase Ib/randomized phase II in patients with unresectable PDAC and eligible to receive first-line chemotherapy, we

[1]Digestive Molecular Clinical Oncology Research Unit, Università degli studi di Verona, Verona, Italy. [2]Investigational Cancer Therapeutics Clinical Unit, Azienda Ospedaliera Universitaria Integrata, Verona, Italy. [3]iOnctura SA, Geneva, Switzerland.

S. Pietrobono and F. Sabbadini contributed equally to this article.

Corresponding Author: Davide Melisi, University of Verona, AOUI Policlinico, Verona 37134, Italy. E-mail: davide.melisi@univr.it

Cancer Res 2024;84:118–32

doi: 10.1158/0008-5472.CAN-23-0104

demonstrated that the combination of the first-generation TGFβ receptor type-1 (ALK5) inhibitor galunisertib plus gemcitabine improved overall survival (OS) versus gemcitabine monotherapy. More recently, we measured an overall 75% disease control rate with the combination of the next-generation TGFβ receptor type-1 small-molecule inhibitor, LY3200882, plus gemcitabine and nab-paclitaxel in treatment-naïve patients with advanced PDAC (16). While these initial encouraging clinical data pointed toward fibrosis and immune modulation as relevant targets in PDAC, several unanswered and important questions remain. One such question related to the presence of additional stromal signals that might impair the inhibition of TGFβ signaling and consequently represent novel targets for combination strategies.

Autotaxin is a secreted enzyme that hydrolyzes lysophosphatidylcholine to produce lysophosphatidate (LPA), which signals through six different G protein–coupled receptors (17). Autotaxin can be secreted either by cancer cells or by stromal cells, including adipocytes and fibroblasts (18). The autotaxin-LPA signaling axis plays a key role in a wide variety of physiologic and pathologic processes, including cancer cell proliferation, migration, invasion, metastasis, and chemoresistance (19). Recently, transcriptomic profiling of iCAFs and myCAFs revealed autotaxin among those genes that are most significantly upregulated in iCAFs (20).

Here, we hypothesized a role for autotaxin as a relevant stromal signal that might impair the activity of TGFβ inhibition and contribute to the resistance to current therapies in PDAC. Thus, a combination of targeting the autotaxin-LPA axis and TGFβ signaling in conjunction with gemcitabine-based chemotherapy could represent a novel therapeutic strategy for patients with PDAC.

Materials and Methods

Compounds and treatments

Galunisertib and gemcitabine were purchased from Selleckchem (catalog nos. S2230 and S1149, respectively). IOA-289 was kindly provided by iOnctura. For *in vitro* experiments, galunisertib, IOA-289, and gemcitabine were dissolved in 100% DMSO (Applichem) and used at indicated concentrations: 0.78 to 200 nmol/L (gemcitabine), 5 μmol/L (galunisertib), or 10 μmol/L (IOA-289). For *in vivo* treatments, galunisertib and IOA-289 were resuspended in hydroxyethylcellulose (0.25%) and administered via oral gavage for 4 weeks at concentration of 50 mg/kg twice/day for galunisertib, and 10 mg/kg twice/day for IOA-289. Gemcitabine was resuspended in saline solution and administered intraperitoneally at concentration of 75 mg/kg once/week.

Cell lines and culture conditions

Pancreatic cancer cells were kindly provided by Dr. Paola Cappello (University of Turin, Turin, Italy) and Prof. Vincenzo Bronte (University of Verona, Verona, Italy). Cells were established by tumors developed in LSL-$Kras^{G12D/+}$; $p53^{R172H/+}$; $PdxCre^{tg/+}$ (KPC) or LSL-$Kras^{G12D/+}$; $PdxCre^{tg/+}$ (KC) mice (Supplementary Table S1). Cells were cultured in DMEM, containing 10% FBS, 1% penicillin-streptomycin solution (Gibco), and 1% Glutamine (Gibco). Pancreatic stellate cells (PSC) were kindly provided by Dr. David Tuveson (Cold Spring Harbor Laboratory Cancer Center, Cold Spring Harbor, New York), and cultured in DMEM 5% FBS supplemented with 1% penicillin-streptomycin and 1% L-glutamine. For coculture experiments, 5×10^5 PSCs and 5×10^5 PDAC cells were plated in each half of a Petri dish in which a hydrophobic barrier prevents the physical interaction of the two cell lines but allows the communication of the culture media. The day after, the barrier was cut, and medium was replaced with serum-free medium to allow cells to communicate for 48 hours in absence or presence of treatments. All cells were maintained in humidified atmosphere at 37°C in a 5% CO_2 incubator, and tested for *Mycoplasma* contamination monthly.

Quantification of the effect of treatments

Crystal violet assay after 72 hours treatment was used to measure cell viability using a plate reader (Victor X4, PerkinElmer). To obtain the response of cell lines to the combination of gemcitabine plus galunisertib plus IOA-289, 1×10^3 PDAC cells were seeded in 96-well plates with 1×10^3 PSCs growing in the top of transwell membranes, and then treated for 72 hours with DMSO or increasing concentrations of gemcitabine (0.78–200 nmol/L), in presence or absence of a fixed dose of 5 μmol/L galunisertib and/or 6 μmol/L IOA-289. Mean EC_{50} values and 95% confidence intervals (CI) were calculated using GraphPad Prism software (GraphPad Software Inc.).

RNA extraction and real-time qPCR

RNA extraction was performed using PureLink RNA Mini Kit according to manufacturer's instructions and quantified by using Nanodrop 8000. After DNase I treatment (Roche Diagnostics), 500 ng of RNA was reverse transcribed with High-Capacity RNA-to-cDNA Kit (Applied Biosystems). qPCR was carried out at 60°C using PowerUp SYBR Green Master Mix (Thermo Fisher Scientific) on a QuantStudio3 (Applied Biosystems). Primers were designed by using Primer3. Primer sequences are reported in Supplementary Table S2.

Protein extraction and Western blot analysis

Cells were lysed in cold RIPA buffer (ab156034, Abcam) supplemented with protease and phosphatase inhibitors for 30 minutes in ice, and then centrifuged at 14,000 rpm for 20 minutes at 4°C. Supernatant was collected and protein quantification was performed using the Pierce BCA Protein Assay Kit (Thermo Fisher Scientific). Equal amounts of protein lysates were loaded onto a 10% polyacrylamide gel, transferred onto nitrocellulose membranes, and incubated for 1 hour in 5% nonfat dry milk at room temperature. Primary antibodies are reported in Supplementary Table S3. Blotted membranes were developed by using Immobilon Western Chemiluminescent horseradish peroxidase (HRP) Substrate (Merck Millipore) and imaged with UVITEC Alliance Q9 Advanced (UVITEC Cambridge).

Nonradioactive electrophoretic mobility shift assay

Electrophoretic mobility shift assay (EMSA) for NFκB was performed with the SYBR Green & SYPRO Ruby EMSA stain kit (E33075) according to the manufacturer's instructions. (catalog no. E33075, Thermo Fisher Scientific). Briefly, cells were lysed in ice-cold cytoplasmic Buffer A added with protease and phosphatase inhibitors for 10 minutes. Lysates were centrifugated at 2,000 × *g* for 5 minutes, supernatant discarded, and nuclear pellet was then lysed in 70 μL buffer C added with protease and phosphatase inhibitors for 30 minutes. For oligomer duplexes, 500 nmol/L of each of the two complementary oligonucleotides was mixed in a total volume of 100 μL of binding buffer. Complementary oligonucleotides were NFκB F: 5′-AGTTGAGGGGACTTTCCCAGGC-3′ and NFκB R: 5′-GCCTGGGAAAGTCCCCTCAACT-3′. After 10 minutes incubation at 95°C followed by additional 15 minutes at 70°C, samples were left to form oligomer duplexes while gradually cooling to room temperature. A total of 20 μg of nuclear extract were then added in binding buffer for additional 30 minutes at room temperature. Protein–DNA complexes were resolved by native 4% PAGE. Nucleic acid staining was achieved by incubating gel with SYBR Green EMSA gel stain solution in shaking

for 20 minutes. Nucleic acids were visualized using UVITEC Alliance Q9 Advanced (UVITEC Cambridge).

Chromatin immunoprecipitation

A total of 5×10^5 PSCs and 5×10^5 RC416, FC1199, or B6KPC cells were plated in a 150 mm dish separated by a hydrophobic barrier and let to attach overnight. The day after, medium was replaced with serum-free DMEM to allow cells to communicate for 48 hours in absence or presence of treatments. For chromatin immunoprecipitation (ChIP) experiments (7), RC416 were fixed with 1% formaldehyde for 15 minutes, followed by addition of 125 mmol/L glycine for 5 minutes to stop fixation. Cells were lysed in Farnham lysis buffer (5 mmol/L PIPES pH 8, 85 mmol/L KCl, 0.5% NP-40) supplemented with phosphatase and protease inhibitors for 20 minutes. Nuclei were collected by centrifugation at $800 \times g$ for 10 minutes and then lysed in nuclear lysis buffer (1% SDS, 10 mmol/L EDTA, 50 mmol/L Tris-HCl pH 8) supplemented with phosphatase and protease inhibitors. Chromatin was sonicated to an average size of 200–500 bp with an ultrasonic bath, diluted with ChIP Dilution Buffer (10 mmol/L Tris-HCl pH 8, 2 mmol/L EDTA, 140 mmol/L NaCl, 1% Triton X-100, 0.1% SDS) and incubated overnight with 20 μL protein G magnetic dynabeads and 3 μg of rabbit anti NFκB (D14e12; #8242, Cell Signaling Technology, 1:300) or normal rabbit IgG (#2729, Cell Signaling Technology, 1:300). Immunocomplexes were washed with increasing salt concentrations, DNA was eluted at 65°C with 1% SDS and recovered with QIAquick PCR Purification Kit (Qiagen). qPCR was carried out at 60°C using PowerUp SYBR Green Master Mix (Thermo Fisher Scientific) on a QuantStudio3 (Applied Biosystems). Promoter sequence of Cxcl1 has been obtained at UCSC Genome Browser GRCm38/mm10 (chr5:90887842-90889342). Primer sequences are reported in Supplementary Table S2.

ELISA

ELISAs were performed with mouse Enpp2 Immunoassay (catalog no. EM0549, FineTest) and Human ENPP-2/autotaxin Quantikine ELISA Kit (catalog no. DENP20, R&D System). Plasma samples were diluted 1:50 (mice) or 1:20 (human) before use. Reagents and standard dilutions were prepared according to manufacturer's instructions. The optical density was determined with the microplate reader iMark (Bio-Rad) at 540 nm. All patients provided written informed consent, and the protocol was approved by the ethics committee of the Azienda Ospedaliera Universitaria Integrata di Verona. The H9H-MC-JBAJ study was conducted in compliance with Good Clinical Practice guidelines and the Declaration of Helsinki.

In vivo orthotopic transplantations

Five to 6 weeks old C57BL/6J female were purchased from Charles River Laboratories. Murine PDAC cells were resuspended in a PBS: Matrigel solution (1:1) at the concentration of 1×10^5 cells per 40 μL/injection. On day 0, mice were anesthetized by exposure to isoflurane and injected orthotopically into the pancreas parenchyma as previously described in ref. 21. Mice bearing pancreatic cancer were randomly allocated into eight groups ($n = 10$) to receive IOA-289 (10 mg/kg), galunisertib (50 mg/kg), gemcitabine (75 mg/kg) or their vehicle for 4 weeks. Half of animals ($n = 5$) were euthanatized at the end of treatments for the analysis of stromal cell composition, whereas the remaining ones ($n = 5$) at cutoff, when tumor volumes reached 1,500 mm^3. Peripheral blood was collected by retro-orbital sinus puncture, and tumors collected for *ex vivo* analysis. All animal studies have been approved by the Institutional Animal Care and Use Committee of University of Verona (Verona, Italy) and by the Italian Ministry of Health (authorization no. 299/2022-PR), and conducted in accordance with Italian Governing Law (D.lgs 26/2014). For *in vivo* experiments, mice were maintained at the animal facility (Centro Interdipartimentale di Servizio alla Ricerca Sperimentale, CIRSAL) of University of Verona (Verona, Italy). Animals were maintained in a pathogen-free and temperature-controlled environment, with 12 hours light and dark cycles, housed in plastics cages and were fed *ad libitum*. The Body Condition Scoring was used to assess mice health status (22).

Flow cytometry

For flow cytometric analysis, tumor samples ($n = 5$) were explanted at the end of treatments, and dissociated using tumor dissociation kit mouse (catalog no. 130-096-730, Miltenyi Biotec) according to manufacturer's instructions. iCAF and myCAF subpopulations were addressed using the following antibodies: CD45-APC-Vio770 (REA737), CD326/EpCAM-APC (REA977), Ly6c-FITC (REA796; Miltenyi Biotec), and Pdpn-PE (127407; BioLegend). MDSCs and CD8 phenotype were evaluated with the following antibodies: CD45-APC-Vio770 (REA737), CD11b-APC (REA592), Ly6c-FITC (REA796), Ly6g-PE-Vio770 (REA526), CD3-PerCP-Vio700 (REA641), CD8-Vioblue (REAL187), CD178 Pe-Vio615 (REA1171) and the Fixable die Viobility 405/520, all from Miltenyi Biotec. Acquisition was performed using Becton Dickinson LSR-Fortessa X-20, and samples were analyzed with FlowJo software (TreeStar Inc.).

IHC and Masson's trichrome

IHC, hematoxylin and eosin (H&E), and Masson's trichrome were performed on murine pancreatic sections of formalin-fixed paraffin-embedded specimens. Sections at 5 μm interval were cut from each tissue and stained with trichrome, H&E (catalog no. H-3502, Vector Laboratories), or via IHC. For IHC, slides were deparaffinized by K-Clear (Kaltek) and rehydrated by ethanol gradient, then heated for 20 minutes at 98°C using BOND Epitope Retrieval Solution (Vector Laboratories) followed by 20 minutes at room temperature. Endogenous peroxidases were quenched in 3% hydrogen peroxide in methanol for 15 minutes. Tissues were blocked with 2.5% BSA blocking solution (Vector laboratories) for 1 hour, and incubated with primary antibodies against NFκB (Cell Signaling Technology), αSMA, Pdpn, and CD8 (Abcam) at 1:200–1:2,000 overnight at 4°C (see Supplementary Table S3). Slides were developed using Immpact DAB (3,3′-diaminobenzidine) substrate peroxidase HRP substrate (Vector Laboratories). Masson's trichrome was performed using Trichrome Stain Kit (catalog no. ab150686, Abcam) according to manufacturer's instructions. Slides were analyzed with ImageJ software.

Multiplex cytokines profiling

Plasma concentration of IL1α, IL1β, IL2, IL3; IL4, IL5, IL6; IL9, IL10, IL12 (p40), IL12 (p70), IL13, IL17a, Eotaxin, GCSF, GMCSF, IFNγ, keratinocyte-derived Chemokine (KC/CXCL1), monocyte chemoattractant protein (MCP1), macrophage inflammatory protein 1α (MIP-1α), MIP1-β, Rantes and TNFα were measured by using a 23-plex Luminex kit (#M60009RDPD, Bio-Rad) according to the manufacturer's instructions. Median fluorescence intensities were collected on a Bio-plex 200 instrument, using Bio-Plex Manager software (version 6.2). Standard curves were generated using the premixed lyophilized standards provided in the kit. Plasma concentration of each cytokine was determined from the standard curve using a 5-point regression to transform mean fluorescence intensities into concentrations.

Statistical analysis

Data represent mean ± SD or mean ± 95% CI values calculated on at least three independent experiments. *P* values were calculated using Student *t* test (two groups) or one-way ANOVA with Dunnett or Tukey corrections (more than two groups). A two-tailed value of $P < 0.05$ was considered statistically significant. *, $P < 0.05$; **, $P < 0.01$; ***, $P < 0.0001$. We used a linear mixed model to analyze the concentration of autotaxin in human plasma at baseline and after 60 days of treatment with gemcitabine plus placebo or gemcitabine plus galunisertib. Progression-free survival was estimated by using the Kaplan–Meier method and a log-rank test was used to compare the results between groups. Statistical analyses were performed using GraphPad Prism version 9 and R version 4.2.2 (R Foundation for Statistical Computing. URL https://www.R-project.org/).

Data and materials availability

Summary data associated with this study are available in the article and its Supplementary Data. All raw data generated in this study are available upon request from the corresponding author.

Results

iCAFs produce autotaxin in response to TGFβ receptor inhibition

Initially, we analyzed orthotopic models from ten different murine PDAC cell lines established by tumors developed in LSL-$Kras^{G12D/+}$; $p53^{R172H/+}$; $PdxCre^{tg/+}$ (KPC) or LSL-$Kras^{G12D/+}$; $PdxCre^{tg/+}$ (KC) mice (Supplementary Table S1) to identify those models with the higher activation of TGFβ pathway. On the basis of their survival, we observed two groups of models, one with a longer median OS (mOS) duration including DT4313, DT6606, and PAN610 tumors, and a more aggressive one with a shorter mOS duration including FC1245, FC1199, CR705, PANC02, B6PKC, K8484, and RC416 tumors (**Fig. 1A**). Among the most aggressive models, mice bearing RC416, FC1199, and B6KPC tumors had the highest plasma levels of ligand Tgfβ1 (**Fig. 1B**), higher infiltration of αSMA–positive (αSMA^+) myCAFs (**Fig. 1C** and **D**) and an increased collagen deposition measured by Masson's trichrome staining (**Fig. 1E**).

To evaluate the effect of targeting TGFβ pathway in these models, mice bearing orthotopic tumors established by injecting five different murine PDAC cell lines were randomly assigned to be treated with galunisertib, or its oral vehicle as control ($n = 6$). We did not measure any difference between the treatment arms in terms of mOS duration (**Fig. 2A**; Supplementary Fig. S1A) or tumor volume (**Fig. 2B**; Supplementary Fig. S1B). However, treatment with galunisertib modulated the phenotype of CAFs by significantly ($P < 0.05$) increasing the rate of $EpCAM^-/Pdpn^+/Ly6C^+$ iCAFs and decreasing that of $EpCAM^-/Pdpn^+/Ly6C^-$ myCAFs (**Fig. 2C**; Supplementary Fig. S1C), while recruitment of total CAFs was not affected (**Fig. 2D**; Supplementary Fig. S1D). Tumors from mice treated with galunisertib had a lower infiltration of Pdpn-positive, αSMA–high myCAFs than untreated controls (**Fig. 2E–G**; Supplementary Fig. S1E–S1G).

To explore our hypothesis about a potential role for autotaxin in impairing the activity of TGFβ inhibition, we evaluated plasmatic levels of autotaxin in mice bearing RC416, FC1199, B6KPC, DT6606, or DT4313 tumors treated with galunisertib and in untreated controls. Importantly, mice treated with galunisertib had significantly higher ($P < 0.01$) plasmatic levels of autotaxin than did vehicle-treated controls (**Fig. 3A**).

To gain insights into the cellular and molecular mechanisms responsible for the activation of the autotaxin pathway upon inhibition of TGFβ signaling in PDAC, we used coculture models in which a hydrophobic barrier allows paracrine interactions between tumor cells and PSCs, one of the recognized precursors of CAFs in PDAC (1), but prevents direct contact between these two cell types (**Fig. 3B**). By using this model, we detected higher levels of Smad2 phosphorylation in PSCs when cocultured with different PDAC cell lines. This activation of TGFβ signaling was completely suppressed by galunisertib (**Fig. 3C**; Supplementary Fig. S2A).

Consistent with the phenotype switch observed *in vivo*, galunisertib significantly ($P < 0.001$) increased the expression of the iCAF markers Il6, *Ly6C* and *Il1a*, and reduced the myCAF markers *Acta2* and *Tagln* in CAFs precursor PSCs when cocultured with FC1199, B6KPC, RC416, DT4313, or DT6606 PDAC cells (**Fig. 3D** and **E**; Supplementary Fig. S2B and S2C). Gene expression analysis revealed that PSCs had higher levels of the autotaxin coding gene *Enpp2* than did all the different PDAC cells as single culture. Most importantly, Enpp2 expression was significantly increased by coculture only in PSCs, but not in any of the PDAC cell lines. Of note, treatment with galunisertib induced a further significant increase of *Enpp2* only in PSCs when cocultured with tumor cells (**Fig. 3F**; Supplementary Fig. S2D). Consistently, treatment with galunisertib led to a significantly higher secretion of autotaxin in conditioned media collected from PSCs when in coculture with any PDAC cell line (**Fig. 3G**).

These results demonstrated that treatment with galunisertib modulates PSCs by skewing them toward an iCAF phenotype within the tumor microenvironment. These iCAFs are the major source of autotaxin, which is overexpressed as an early adaptive mechanism in response to TGFβ pathway inhibition.

Targeting autotaxin hampers the resistance to TGFβ receptor inhibition and gemcitabine sustained by NFκB

To study the involvement of autotaxin in the resistance of PDAC to galunisertib and classic chemotherapeutic agents, we used IOA-289, a potent, selective autotaxin inhibitor, which has been developed as a novel treatment for highly fibrotic tumors (23, 24). We initially measured the expression of the most relevant LPA receptors *Lpar1, 2*, and *4* in PSCs and in different tumor cell lines. While *Lpar1* and *4* were mostly expressed in PSCs, Lpar2 was the main receptor on murine PDAC cell lines (**Fig. 4A**). When cocultured with PSCs, we measured a significant activation of several intracellular pathways known to be activated by the autotaxin-LPA axis, including Erk1/2, p38, Stat3, and NFκB in RC416, FC1199, and B6KPC murine PDAC cell lines (25). Autotaxin inhibitor IOA-289 significantly decreased the phosphorylation of these proteins (**Fig. 4B**). Consistently with the known profibrotic activity of autotaxin-LPA axis (26), IOA-289 treatment of PSCs significantly decreased the expression of myCAFs markers *Acta2* and *Tagln* (**Fig. 4C**), while increased that of iCAF markers *Il1a*, *Ly6c* only when cocultured with PDAC cells (**Fig. 4D**). This skewing of PSCs toward an iCAF phenotype was significantly boosted by the combined inhibition of TGFβ and autotaxin pathways (**Fig. 4C** and **D**).

The transcriptional factor NFκB is among the most important mediators of treatment resistance in patients with PDAC (27). We measured a significant activation of NFκB in RC416, B6KPC, and FC1199 tumor cells upon treatment with galunisertib only when cocultured with iCAFs. Importantly, treatment with IOA-289 completely reverted the phosphorylation of NFκB (**Fig. 5A**), as well

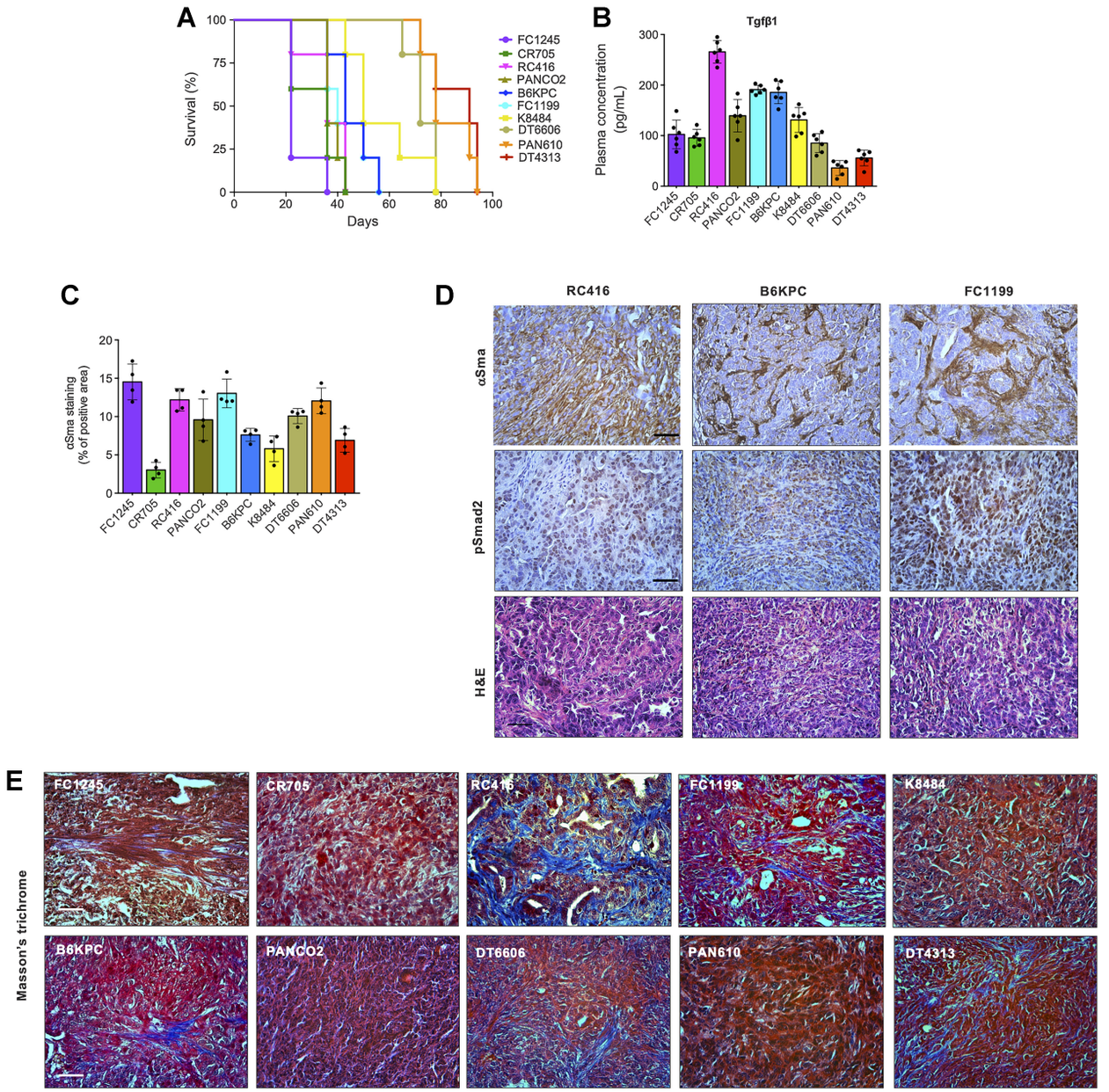

Figure 1.

Characterization of orthotopic murine PDAC tumors. **A,** mOS of C57BL/6J mice orthotopically injected with 10 murine PDAC cell lines. **B,** Plasma levels of Tgfβ1 ligand measured in tumor-bearing mice using ELISA. Data are expressed as mean ± SD ($n = 5$). **C,** Quantification of paraffin sections from 10 orthotopic murine PDAC tumors stained with αSMA antibody. Data are expressed as mean ± SD ($n = 4$). **D,** Representative images for RC416, FC1199, and B6KPC tumors stained with αSMA antibody and H&E. Scale bar, 60 μm. **E,** Masson's trichrome staining of orthotopic tumors from 10 murine PDAC cells showing collagen deposition in RC416 tumors. Scale bar, 60 μm.

as its nuclear translocation and promoter binding induced by galunisertib (**Fig. 5B**).

Then, we evaluated the effect of the combined targeting of TGFβ and autotaxin signaling on the *in vitro* response to the chemotherapeutic agent gemcitabine in five different murine PDAC cell lines, RC416, B6KPC, FC1199, DT4313, and DT6606, when cocultured with PSCs. Single agents galunisertib or IOA-289 had only a moderate effect in potentiating the antitumor activity of gemcitabine, whereas the combined treatment with IOA-289 plus galunisertib led to a measurable reduction in the EC_{50} of gemcitabine in all PDAC cells in coculture with PSCs (**Fig. 5C**).

To evaluate the therapeutic potential of the combined targeting of TGFβ plus autotaxin signaling with standard chemotherapy *in vivo*, mice bearing orthotopic RC416 tumors were randomly assigned to be treated with the single-agent gemcitabine, galunisertib or IOA-289, their double combinations, the three agents combined, and their

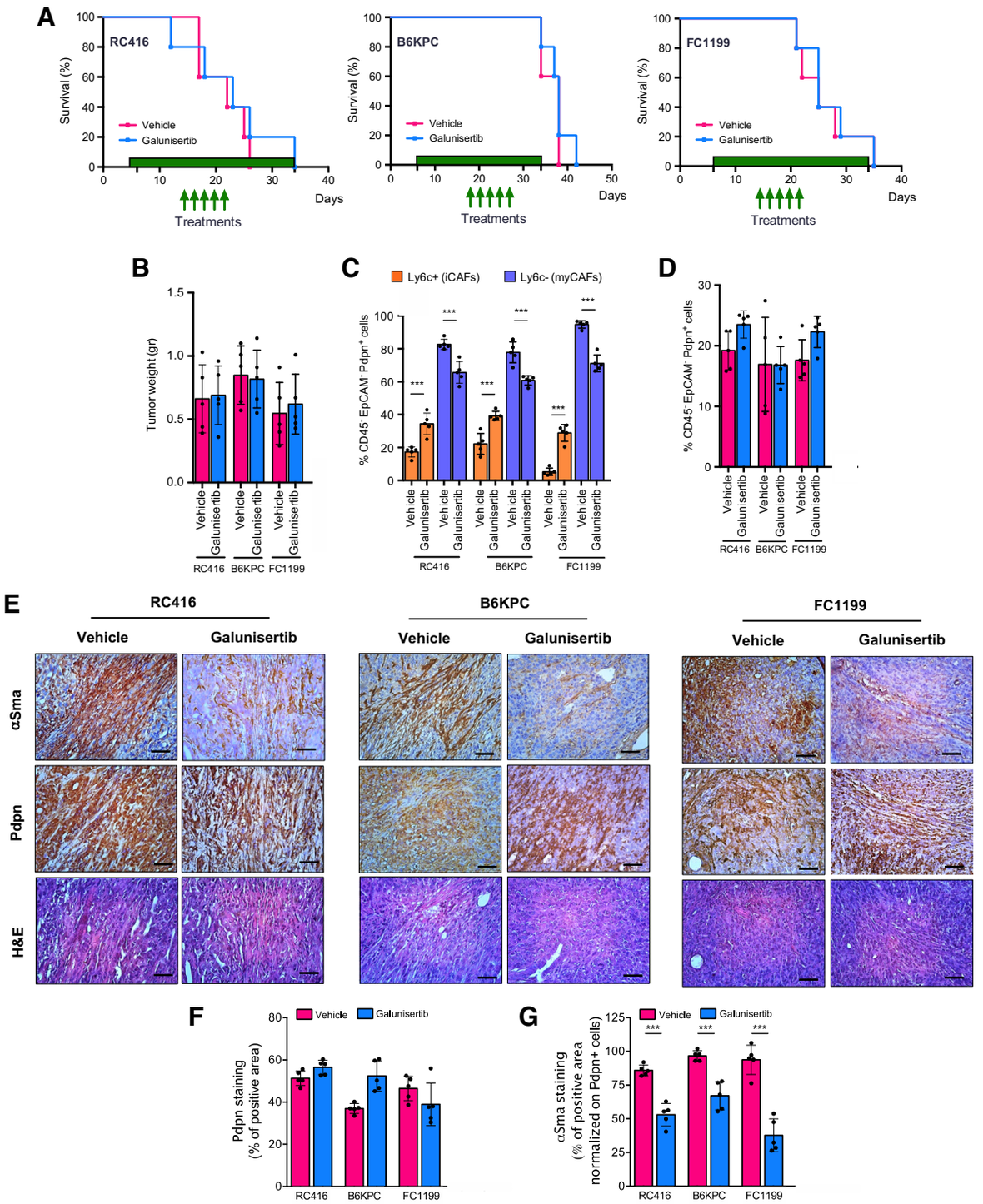

Figure 2.

TGFβRI inhibition sustains an inflammatory phenotype of CAFs (iCAF). **A** and **B,** mOS duration (**A**) and tumor volume (**B**) of RC416, FC1199, and B6KPC tumor-bearing mice treated for 4 weeks with galunisertib or its oral vehicle as control. The mean values and SD are shown ($n = 5$). **C** and **D,** Flow cytometry analysis of RC416, FC1199, and B6KPC tumor samples showing increased iCAF (EpCAM$^-$/PDPN$^+$/LY6c$^+$)/myCAF (EpCAM$^-$/PDPN$^+$/LY6c$^-$) ratio upon administration of galunisertib (**C**), whereas total CAFs recruitment (**D**) was not affected. Data are expressed as mean ± SD. *P* value was calculated by two-tailed unpaired Student *t* test ($n = 5$). **E,** Representative images of paraffin sections from murine RC416, FC1199, and B6KPC orthotopic tumors treated as indicated and stained with Pdpn or αSMA antibodies. **F** and **G,** Quantification of Pdpn stain (**F**) and of αSma$^+$/Pdpn$^+$ myCAFs (**G**) in RC416, FC1199, and B6KPC paraffin sections treated as indicated. Data are expressed as mean ± SD. *P* value was calculated by two-tailed unpaired Student *t* test ($n = 5$). Scale bar, 150 μm. ***, $P < 0.001$.

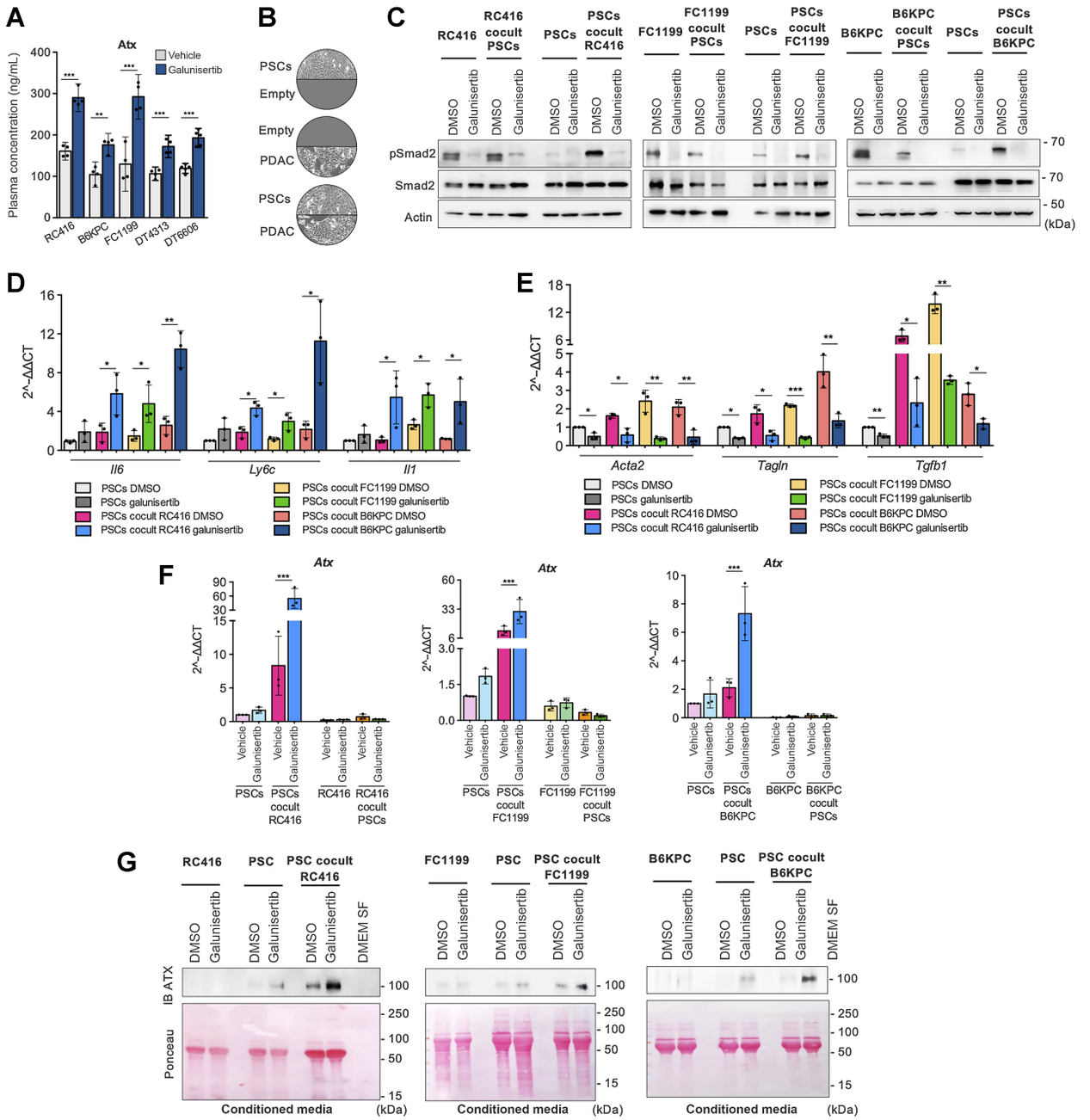

Figure 3.

TGFβRI inhibition increases secretion of autotaxin from iCAFs. **A,** Plasma levels of autotaxin measured by ELISA in RC416, FC1199, B6KPC, DT4313, and DT6606 orthotopic tumors treated as indicated. Data are expressed as mean ± SD. *P* value was calculated by two-tailed unpaired Student *t* test ($n = 4$). **B,** Schematic representation of the coculture technique used to culture PSCs and pancreatic cancer cells physically separated by a hydrophobic barrier but in the same culture medium. **C,** Representative Western blot of pSmad2 and Smad2 in PSCs and RC416, FC1199, or B6KPC treated as indicated, confirming the efficacy of TGFβ inhibition. Actin was used as loading control. **D** and **E,** qPCR analysis of iCAF markers (*Il6, Ly6c, Il1a*; **D**) and myCAF markers (*Acta2, Tagln, Tgfb1*; **E**) in PSCs as single cultures or cocultured with RC416, FC1199, or B6KPC and treated with DMSO or 5 μmol/L galunisertib for 24 hours. Results show mean ± SD of three biological replicates. *P* value was calculated by two-tailed unpaired Student *t* test. **F,** qPCR of *Enpp2* in PSCs and RC416, FC1199, or B6KPC cells as single cultures or in coculture. Results show mean ± SD of three biological replicates. *P* value was calculated by ANOVA and Tukey test. **G,** Representative Western blot of secreted autotaxin in the conditioned media of PSCs and RC416, FC1199, or B6KPC cells as single cultures or in coculture. SF, serum-free. *, $P < 0.05$; **, $P < 0.01$; ***, $P < 0.001$.

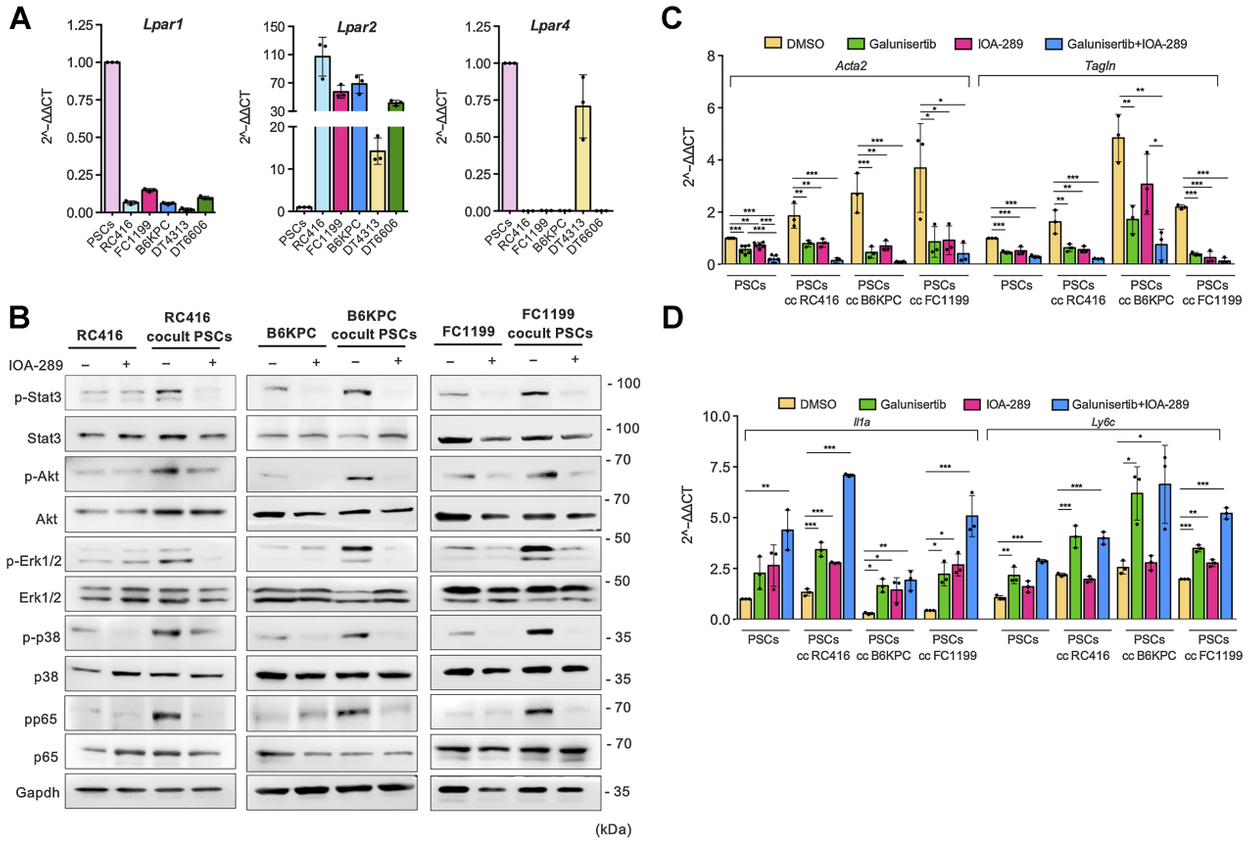

Figure 4.

IOA-289 is a potent inhibitor of the myofibroblastic phenotype of CAFs. **A,** qPCR of *Lpar1*, *Lpar2*, *Lpar4* in PSCs and in a panel of PDAC cell lines. **B,** Representative Western blot analysis of the indicated proteins in RC416, B6KPC, and FC1199 as single cultures or cocultured with PSCs and treated with 6 μmol/L IOA-289. Gapdh was used as loading control. **C** and **D,** qPCR analysis of myCAF markers (*Acta2, Tagln*; **C**) and iCAF markers (*Il1a, Ly6c*; **D**) in PSCs as single cultures or cocultured with RC416, FC1199, or B6KPC and treated with DMSO, 5 μmol/L galunisertib, and 6 μmol/L IOA-289 alone or in combination for 24 hours. *, $P < 0.05$; **, $P < 0.01$; ***, $P < 0.001$.

respective vehicles as control ($n = 5$). Mice receiving gemcitabine plus IOA-289, or gemcitabine plus galunisertib, showed a significantly longer mOS duration than any single treatment or vehicle control (mOS = 38 days, $P < 0.05$; **Fig. 6A**). Most importantly, mice treated with the triple combination of gemcitabine plus IOA-289 and galunisertib had the longest mOS survival when compared with doublet combination (mOS = 47 days, $P < 0.05$; **Fig. 6A**). All treatments were tolerated in mice (Supplementary Fig. S3A).

In this model, we confirmed that galunisertib induced an iCAF skewing, and demonstrated that its combination with IOA-289 boosted this effect as almost all the $Cd45^-/EpCAM^-/Pdpn^+$ cells in tumors from mice receiving the combination of galunisertib plus IOA-289 were $Ly6C^+$ (**Fig. 6B**). Consistently, the combination of galunisertib plus IOA-289 was the most effective in reducing the infiltration of αSMA^+ myCAFs (**Fig. 6C** and **D**; Supplementary Fig. S3B and S3C), the degree of fibrosis (**Fig. 6E**; Supplementary Fig. S3D), and the plasma levels of connective tissue growth factor (Ctgf; **Fig. 6F**), either alone or in combination with gemcitabine.

Consistently with our *in vitro* data, tumors from mice receiving gemcitabine were characterized by a moderate cytoplasmic staining of NFκB (**Fig. 6C** and **G**). Tumors from mice receiving the combination of gemcitabine plus galunisertib showed a significantly higher NFκB staining, which was observed mainly in the tumor cells nuclei. NFκB nuclear expression was not detected in tumors from mice receiving the combination of gemcitabine plus IOA-289. Most importantly, in the triple combination group, IOA-289 treatment was able to fully rescue the hyperactivation of NFκB induced by galunisertib (**Fig. 6C** and **G**).

Altogether, these results describe a model in which autotaxin is released by iCAFs in response to TGFβ inhibition, which in turn produce LPA that activates NFκB in PDAC cells, contributing to their chemoresistance. Consequently, targeting autotaxin by using IOA-289 suppresses NFκB activation in tumors cells and reduces their resistance to galunisertib and chemotherapeutic agents.

Targeting autotaxin boosts tumor infiltration of $CD8^+$ T lymphocytes by modulating paracrine Cxcl1

To identify circulating biomarkers of activity for IOA-289 in modulating the resistance to TGFβ inhibition, we evaluated the plasma concentration of a panel of 23 different cytokines, chemokines, and growth factors in mice treated with gemcitabine, galunisertib, IOA-289, their doublet combinations, the three agents combined, or their vehicles as control. Among these analytes, we measured a significantly ($P < 0.05$) higher plasma levels of Cxcl1 in mice bearing RC416 and treated with galunisertib, either as single agent or in combination with gemcitabine. Notably, treatment with IOA-289 fully reverted this increase ($P < 0.001$; **Fig. 7A**).

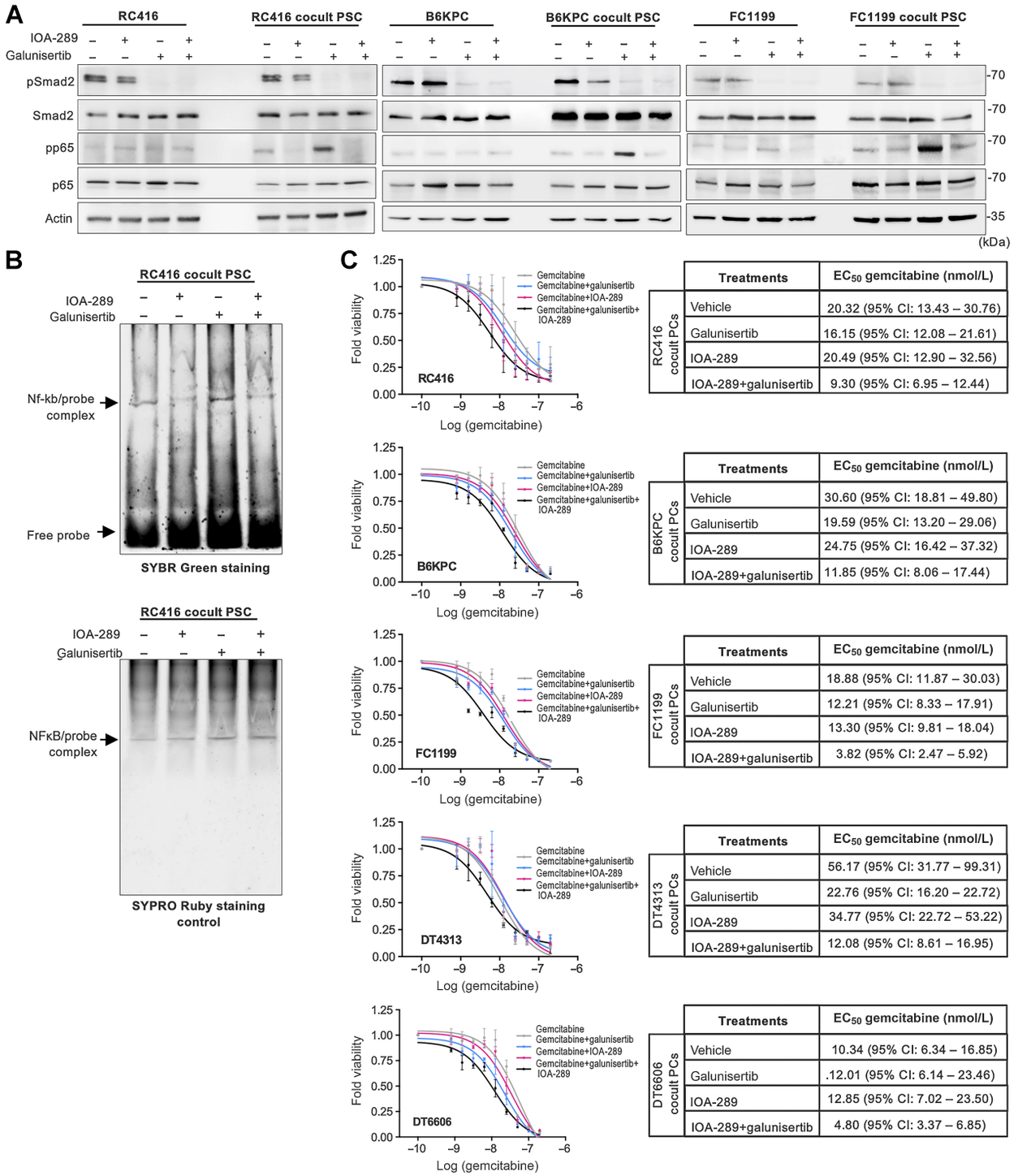

RC416 cocult PCs	Treatments	EC_{50} gemcitabine (nmol/L)
	Vehicle	20.32 (95% CI: 13.43 – 30.76)
	Galunisertib	16.15 (95% CI: 12.08 – 21.61)
	IOA-289	20.49 (95% CI: 12.90 – 32.56)
	IOA-289+galunisertib	9.30 (95% CI: 6.95 – 12.44)

B6KPC cocult PCs	Treatments	EC_{50} gemcitabine (nmol/L)
	Vehicle	30.60 (95% CI: 18.81 – 49.80)
	Galunisertib	19.59 (95% CI: 13.20 – 29.06)
	IOA-289	24.75 (95% CI: 16.42 – 37.32)
	IOA-289+galunisertib	11.85 (95% CI: 8.06 – 17.44)

FC1199 cocult PCs	Treatments	EC_{50} gemcitabine (nmol/L)
	Vehicle	18.88 (95% CI: 11.87 – 30.03)
	Galunisertib	12.21 (95% CI: 8.33 – 17.91)
	IOA-289	13.30 (95% CI: 9.81 – 18.04)
	IOA-289+galunisertib	3.82 (95% CI: 2.47 – 5.92)

DT4313 cocult PCs	Treatments	EC_{50} gemcitabine (nmol/L)
	Vehicle	56.17 (95% CI: 31.77 – 99.31)
	Galunisertib	22.76 (95% CI: 16.20 – 22.72)
	IOA-289	34.77 (95% CI: 22.72 – 53.22)
	IOA-289+galunisertib	12.08 (95% CI: 8.61 – 16.95)

DT6606 cocult PCs	Treatments	EC_{50} gemcitabine (nmol/L)
	Vehicle	10.34 (95% CI: 6.34 – 16.85)
	Galunisertib	.12.01 (95% CI: 6.14 – 23.46)
	IOA-289	12.85 (95% CI: 7.02 – 23.50)
	IOA-289+galunisertib	4.80 (95% CI: 3.37 – 6.85)

Figure 5.

Autotaxin blunts the efficacy of galunisertib and gemcitabine by activating NFκB. **A,** Representative Western blot analysis of pSmad2, Smad2, p-NFκB, and NFκB in RC416, B6KPC, or FC1199 as single cultures or cocultured with PSCs and treated as indicated. Actin was used as loading control. **B,** Nonradioactive EMSA of endogenous NFκB using unconjugated κB oligonucleotides in RC416 cocultured with PSCs and treated as indicated. Gel was stained with SYBR Green EMSA stain (left), followed by SYPRO Ruby EMSA stain (right). The NFκB/probe complex is observed in both DNA and protein staining. **C,** Dose–response curves of RC416, B6KPC, FC1199, DT4313, and DT6606 cocultured with PSCs after 72 hours of treatment with gemcitabine alone, in presence of IOA-289, galunisertib, or their combination at the following concentrations: IOA-289 at 6 mmol/L and galunisertib at 5 mmol/L. Tables indicate EC_{50} values and 95% CIs of gemcitabine.

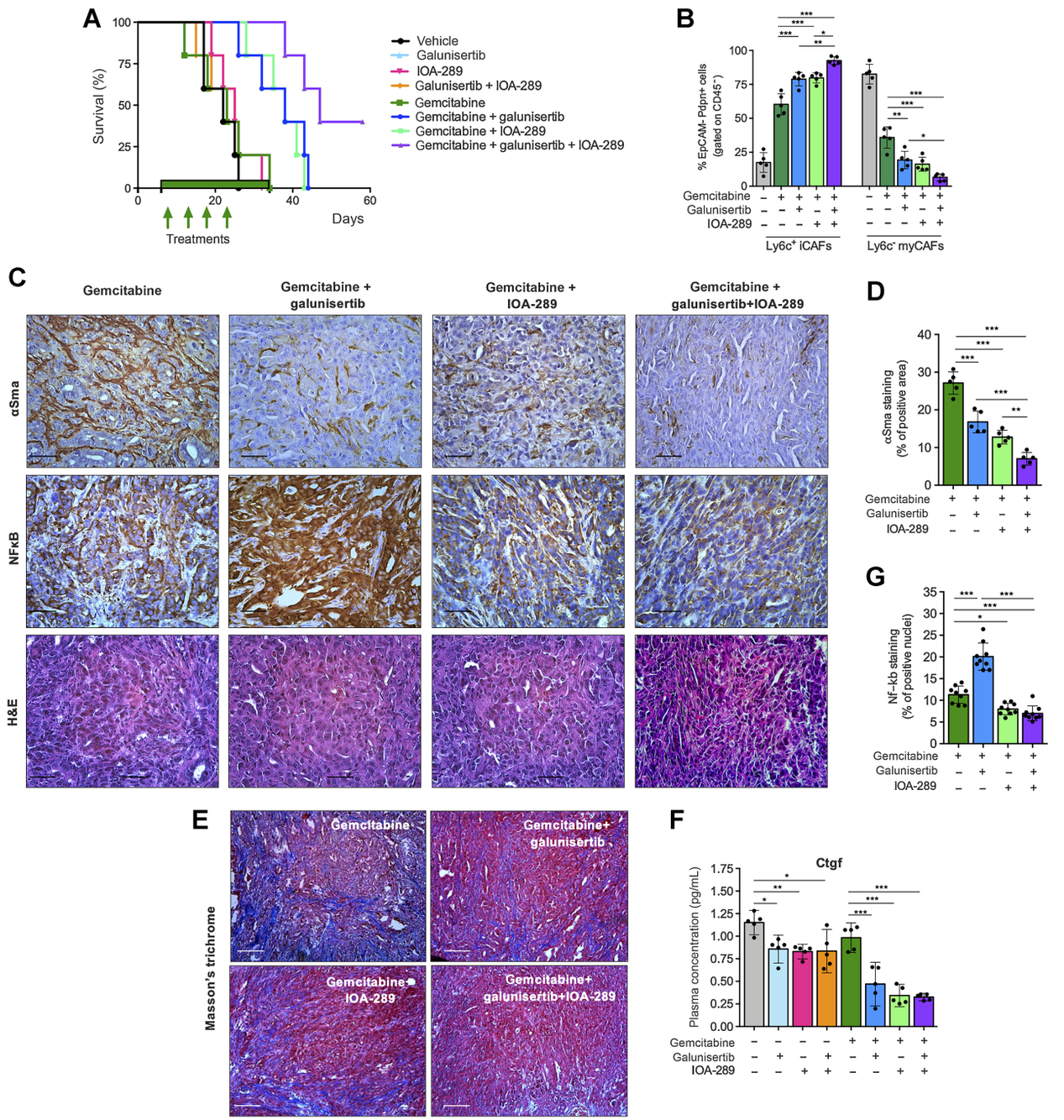

Figure 6.

Combined inhibition of autotaxin and TGFβRI potentiates the efficacy of chemotherapy *in vivo*. **A,** mOS of mice bearing RC416 orthotopic tumors treated with gemcitabine, galunisertib, IOA-289, their double combinations, the three agents combined, or their respective vehicles as control ($n = 5$; mOS gemcitabine plus IOA-289 or gemcitabine plus galunisertib = 35 days, $P < 0.05$; mOS gemcitabine plus IOA-289 and galunisertib triple combination = 47 days, $P < 0.05$). **B,** Flow cytometry analysis of RC416 tumor samples showing increased iCAF ($EpCAM^-/PDPN^+/LY6c^+$)/myCAF ($EpCAM^-/PDPN^+/LY6c^-$) ratio upon administration of both galunisertib and IOA-289. **C,** Representative images of paraffin sections from RC416 tumors treated as indicated and stained with NFκB or αSMA antibodies. Scale bar, 60 μm. **D,** Quantification of paraffin sections from RC416 tumors stained with αSMA antibody. **E,** Quantification of NFκB-positive nuclei in RC416 paraffin sections treated as indicated. **F,** Masson's trichrome staining of RC416 tumor-bearing mice treated as indicated. **G,** Plasma levels of Ctgf measured by ELISA in RC416 orthotopic tumors treated as indicated. Data in **B, D, E,** and **G** are expressed as mean ± SD ($n = 5$). *P* values were calculated by ANOVA and Tukey test. *, $P < 0.05$; **, $P < 0.01$; ***, $P < 0.001$.

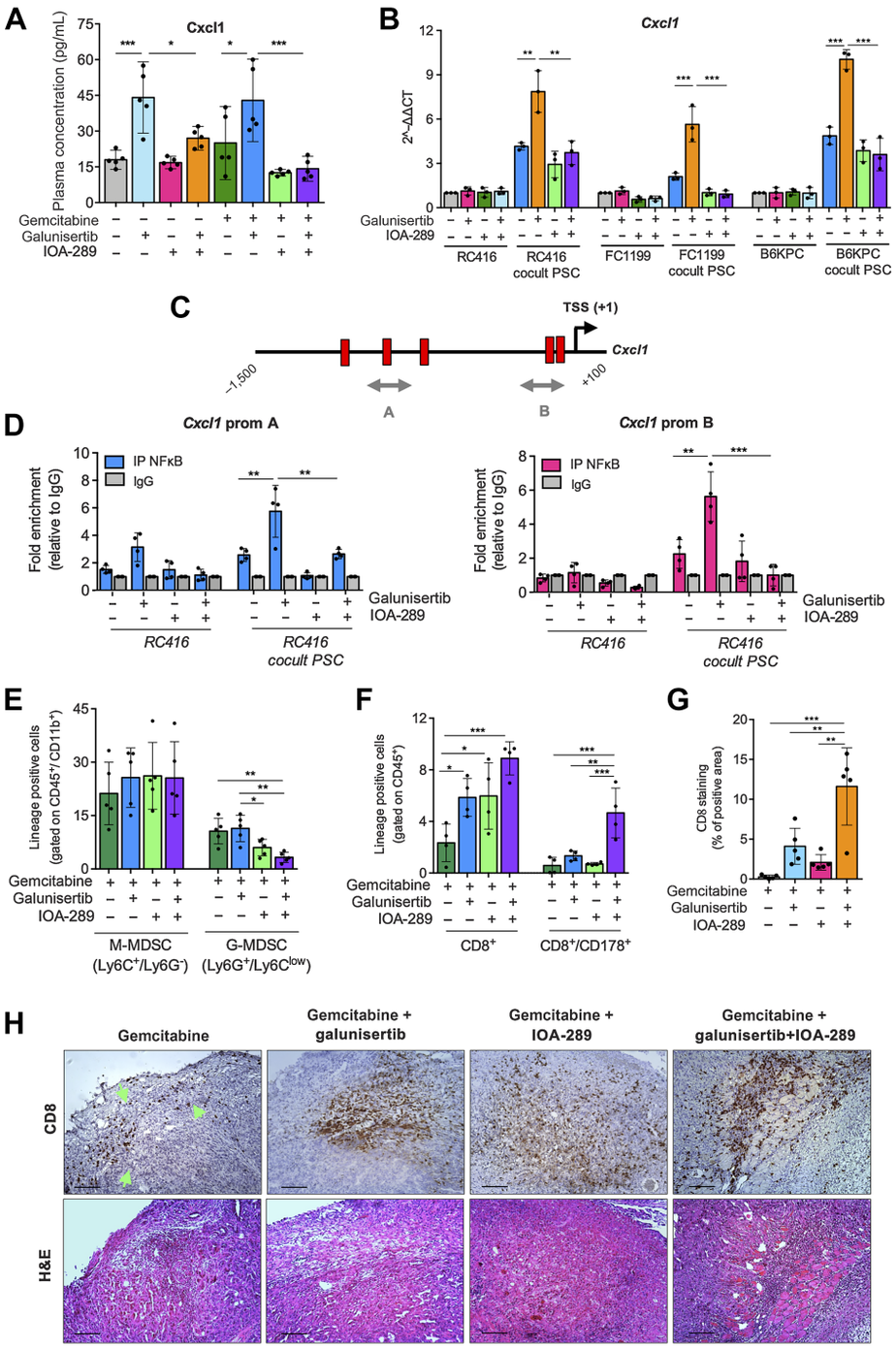

Figure 7.

The autotaxin-NFκB-Cxcl1 axis impairs TGFβ inhibition by recruiting MDSCs while inhibiting cytotoxic CD8$^+$ T-cell infiltration. **A,** Histogram shows Cxcl1 plasmatic concentration in mice inoculated with RC416 cells and treated as indicated. Means and SD ($n = 5$) are shown. *P* value was calculated by ANOVA and Tukey test. **B,** qPCR of Cxcl1 in RC416, FC1199, and B6KPC cells as single cultures or in coculture with PSCs. Data are represented as mean ± SD ($n = 3$). *P* value was calculated by ANOVA and Tukey test. **C,** Schematic representation of Cxcl1 promoter (available at UCSC Genome Browser GRCm38/mm10, chr5:90887842-90889342) with the position of ChIP probes (gray double arrowhead) and consensus NFκB binding sites (vertical slashes) relative to the transcription start site (TSS). **D,** ChIP-qPCR of NFκB occupancy at the *Cxcl1* promoter. The *y*-axis represents relative promoter enrichment, normalized on input material. IgG was set to 1. Data are represented as mean ± SD ($n = 3$). **E,** Flow cytometry analysis of CD45$^+$/CD11b$^+$/Ly6C$^+$/Ly6G$^-$ monocytic (M)-MDSCs and CD45$^+$/CD11b$^+$/LY6g$^+$/LY6c^{low} granulocytic (G)-MDSCs in RC416 tumor samples treated as indicated. **F,** Flow cytometry analysis of CTLs (CD45$^+$/CD3$^+$/CD8$^+$/CD178(FasL)$^+$) in RC416 tumor samples treated as indicated. Data in **E** and **F** are represented as mean ± SD ($n = 4$). **G** and **H,** Quantification (**G**) and representative images (**H**) of CD8$^+$ T lymphocytes in paraffin sections from RC416 tumors treated as indicated. Scale bar, 150 μm. *P* values in **A, B, D, E,** and **F** were calculated by ANOVA and Tukey test. *, $P < 0.05$; **, $P < 0.01$; ***, $P < 0.001$.

By using coculture models of RC416, FC1199, or B6KPC tumor cells with PSCs, we detected a significant upregulation of *Cxcl1* mRNA in tumor cells only when cocultured with PSCs and treated with galunisertib. Consistently with what observed *in vivo*, IOA-289 significantly reduced this expression (**Fig. 7B**).

Cxcl1 expression in tumors is induced by numerous mechanisms, including the activation of transcription by high basal NFκB activation (28). Thus, we studied whether autotaxin-mediated NFκB activation can directly regulate the expression of Cxcl1. ChIP assay using NFκB antibody followed by qPCR with primers spanning different regions of the *Cxcl1* promoter reporting the consensus sequence 5′-GGGRNYYYCC-3′ (**Fig. 7C**; ref. 29) revealed a stronger NFκB occupancy at about 600 bp upstream to *Cxcl1* transcription start site, with a 7-fold enrichment in *Cxcl1* signal over ChIP with an isotype IgG ($P < 0.001$) only in PDAC cells cocultured with PSCs and treated with galunisertib (**Fig. 7D**; Supplementary Fig. S4). Most importantly, administration of IOA-289 almost completely reverted NFκB occupancy at *Cxcl1* promoter induced by galunisertib in cocultured RC416, FC1199, or B6KPC. Contrariwise, immunoprecipitation of NFκB in RC416 FC1199 or B6KPC as single cultures showed no significant enrichment (**Fig. 7D**; Supplementary Fig. S4).

Cxcl1 is a prominent chemokine involved in orchestrating inflammatory responses (30). Among other protumorigenic functions, upregulation of Cxcl1 contributes to the recruitment of different inflammatory cell types, including myeloid-derived suppressor cells (MDSC) that sustain the survival of cancer cells (31, 32). MDSCs are defined by their ability to inhibit immune responses, including those mediated by T cells, and are classified into granulocytic/polymorphonuclear MDSCs and monocytic MDSCs based on the expression of distinctive proinflammatory and immunosuppressive pathways (33). To investigate whether and how the combination of galunisertib and IOA-289 could impact tumor immunity, we analyzed the immune cell composition of tumors from treated mice. Examination of the myeloid cell lineage revealed that, whereas $CD11b^+/Ly6C^{hi}/Ly6G^-$ monocytic MDSCs were not affected, $CD11b^+/Ly6G^+/Ly6c^{low}$ granulocytic MDSCs were significantly decreased in mice receiving the combination of gemcitabine plus IOA-289, and that the triple combination was the most effective in reducing the infiltration of these granulocytic MDSCs (**Fig. 7E**; Supplementary Fig. S5). Further analysis of the immune cell infiltrate revealed that treatment with either IOA-289 or galunisertib markedly increased the recruitment of tumor-infiltrating $CD8^+$ T cells (**Fig. 7F–H**) without altering their intrinsic cytotoxicity (**Fig. 7F**; Supplementary Fig. S5). Consistently with the reduction in granulocytic MDSCs, tumors from mice receiving the combination of galunisertib plus IOA-289 showed the highest infiltration of $CD8^+/CD178(FasL)^+$ CTLs if compared with any other treatment group (**Fig. 7F–H**)

Collectively, our results indicate that one of the most significant effects of targeting autotaxin by using IOA-289 is to modulate the overexpression of Cxcl1 sustained by NFκB. IOA-289, in turn, reduced the recruitment of granulocytic MDSCs, while boosting tumor infiltration by $CD8^+$ T lymphocytes.

Plasma levels of autotaxin are increased by galunisertib plus chemotherapy and predict response to this treatment strategy in patients with advanced PDAC

To confirm the clinical relevance of autotaxin as a mechanism of adaptive resistance to the inhibition of TGFβ pathway in PDAC, we measured the circulating levels of autotaxin in the plasma of patients treated in our clinical unit within the randomized phase II H9H-MC-JBAJ study. This analysis was performed in plasma samples collected at baseline and after 60 days of treatment with gemcitabine plus placebo or gemcitabine plus galunisertib.

While the linear mixed model did not show any significant difference in plasmatic level of autotaxin between day 0 and day 60 in patients treated within the control arm of gemcitabine plus placebo (**Fig. 8A**), a significant increase of autotaxin was measured within the experimental arm of gemcitabine plus galunisertib ($P < 0.01$; **Fig. 8B**). Nonetheless, we measured a significant difference in median progression-free survival duration between patients with increased levels of autotaxin and those who had no difference in plasmatic level of autotaxin upon treatment with gemcitabine plus galunisertib (12.9 vs. 5.3 months; $P = 0.03$; **Fig. 8C**).

Collectively, these results confirm the soundness of our preclinical results in patients affected by advanced PDAC. These results confirm that autotaxin is indeed triggered by TGFβ inhibition, and this induction predicts the response to the combination approach of gemcitabine plus galunisertib. This establishes autotaxin as a potential stromal mechanism of adaptive resistance to the combination strategy of chemotherapy with the inhibition of TGFβ patients with advanced PDAC.

Discussion

The identification of novel approaches to target paracrine signaling pathways within the tumor microenvironment that sustain treatment resistance in PDAC remains of utmost relevance. In this study, we identified for the first time autotaxin as a stromal signal that mediates adaptive resistance to the inhibition of TGFβ pathway and represent a novel target for therapeutic combination strategies. We demonstrated that the inhibition of TGFβ signaling by using galunisertib prompts the skewing of CAFs toward an inflammatory iCAF phenotype. iCAFs are, in turn, responsible for a significant overexpression of autotaxin within the tumor microenvironment. This secreted enzyme acts in a paracrine manner to sustain increased LPA-NFκB signaling in tumor cells, driving resistance to galunisertib and the chemotherapeutic agent gemcitabine. Targeting stromal autotaxin by using the novel selective inhibitor IOA-289 synergizes with the TGFβ inhibitor galunisertib in modulating PDAC chemoresistance *in vivo* and boosting $CD8^+$ T lymphocytes tumor infiltration. Most significantly, we confirmed the reliability of our preclinical model in patients enrolled in the randomized phase II H9H-MC-JBAJ study. We demonstrated a significant increase in autotaxin levels only in patients randomly allocated to the experiment arm of galunisertib plus gemcitabine, and not in those receiving placebo plus gemcitabine as control. Moreover, among patients receiving galunisertib plus gemcitabine, those patients with an increase in autotaxin plasmatic levels had a significantly shorter progression-free survival duration that those who had no difference in plasmatic level of autotaxin, confirming that autotaxin is indeed triggered by TGFβ inhibition, and this induction predicts the response to the combination approach of gemcitabine plus galunisertib.

The inhibition of TGFβ signaling remains one of the most promising experimental therapeutic approaches for the treatment of patients affected by advanced PDAC. However, the positive signal for the activity measured in clinical trial for the TGFβ receptor inhibitor galunisertib could be impaired by different mechanisms of intrinsic resistance originated by tumors cells, including the production of cytokines involved in macrophages enrichment, of factors involved in tumor growth and remodeling, or of miRNA regulating genes significantly associated with digestive tract cancers (13).

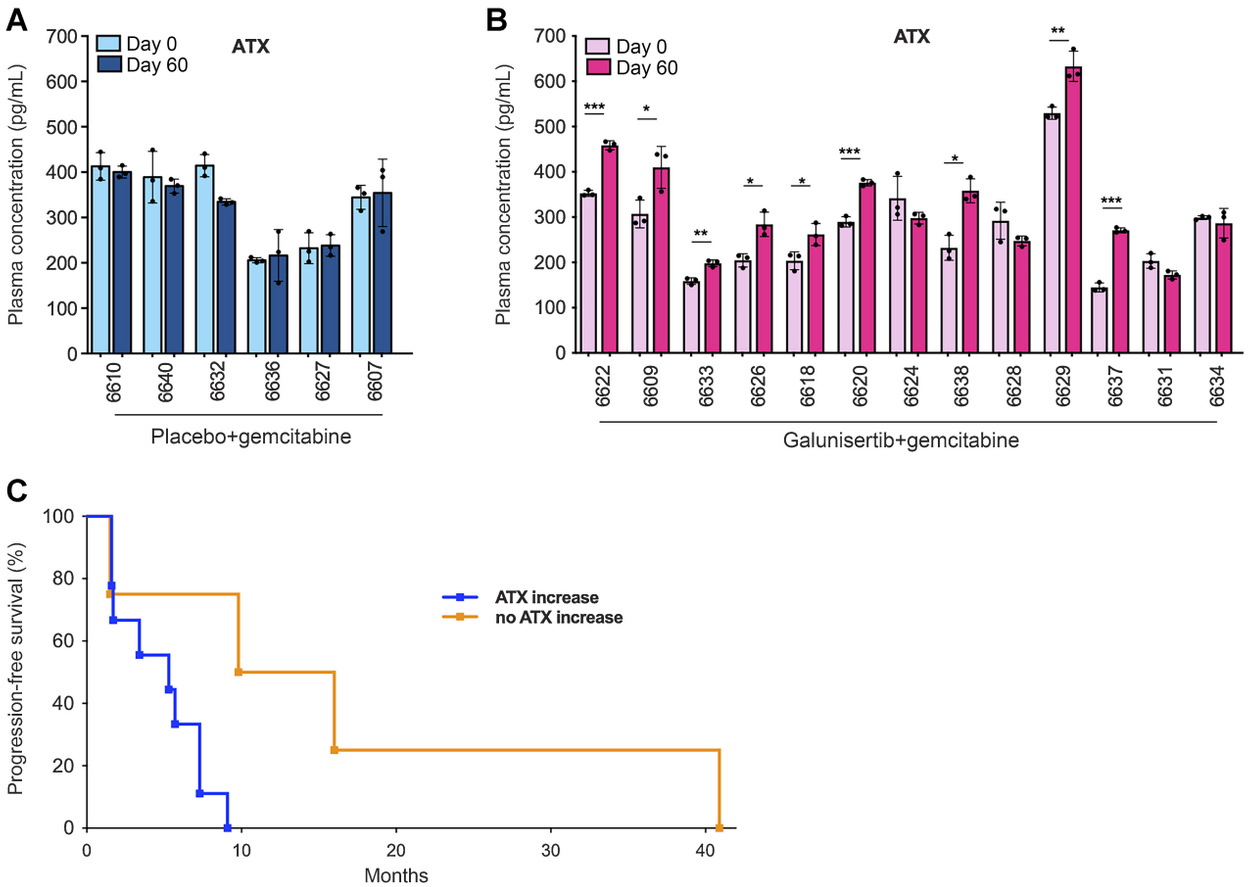

Figure 8.

Plasma levels of autotaxin are increased by galunisertib plus chemotherapy and predict response to this treatment strategy in patients with advanced PDAC. **A** and **B,** Plasma levels of autotaxin measured at baseline (day 0) and after two cycles of treatment (day 60) in patients enrolled in the randomized phase II H9H-MC-JBAJ trial treated with placebo plus gemcitabine as control arm (**A**) or with galunisertib plus gemcitabine as experimental arm (**B**). **C,** Progression-free survival of patients allocated to galunisertib plus gemcitabine, which had a significant increase in plasmatic autotaxin (blue line) versus those with no increase in plasmatic autotaxin (yellow line; 12.9 vs. 5.3 months, $P = 0.03$). *, $P < 0.05$; **, $P < 0.01$; ***, $P < 0.001$.

Nonetheless, acquired stromal signals originated by different cell types in the tumor microenvironment might impair the inhibition of TGFβ signaling by sustaining paracrine protumorigenic pathways. Thus, a deepened understanding of the mechanisms of acquired resistance related to fibroblasts that might limit the efficacy of galunisertib is critical for the development of novel combination strategies. To our knowledge, our study demonstrates for the first time autotaxin as a CAF-mediated mechanism of adaptive resistance to the inhibition of TGFβ receptor in PDAC.

Autotaxin was found to be produced either by tumor or stromal cells within the microenvironment of different human solid tumors (19). In a PDAC *in vitro* model, it has been recently reported that autotaxin is released in similar levels in the conditional medium of PSCs and tumor cells. Autotaxin secretion by PDAC cells was increased by the incubation with the conditional medium of PSCs when compared with incubation with serum-free medium control (34). In our *in vitro* coculture model, which allowed a physiologic dissection of continuous paracrine effects, we demonstrated that iCAFs represent the primary source of autotaxin, rather than PDAC cells. Moreover, we demonstrated that treatment with galunisertib markedly increased within few hours the secretion of autotaxin by iCAFs.

LPA produced by autotaxin signals through at least six different G protein–coupled receptors, which in turn activate the mitogenic signaling of RAS-MAPK and the survival signaling of PI3K-AKT pathways (35). Here we demonstrated a novel relevant molecular mechanism for the autotaxin-LPA axis in sustaining the activation of NFκB in tumor cells. This transcriptional factor significantly contributes to the treatment resistance of solid tumors (27), and PDAC in particular (36). We find that stromal autotaxin activates NFκB through a paracrine mechanism in PDAC cells, and that treatment with the autotaxin inhibitor IOA-289 can prevent phosphorylation and nuclear translocation of NFκB induced in response to the inhibition of TGFβ signaling. Our data suggest that activation of a paracrine autotaxin-NFκB axis upon TGFβ receptor inhibition may limit the efficacy of galunisertib in combination with the chemotherapeutic drug gemcitabine, as treatment with IOA-289 potentiates the efficacy of gemcitabine in combination with galunisertib *in vitro* when PDAC cells were cocultured with PSCs. Of note, the role of autotaxin seems to be dominant in comparison with other paracrine cytokines produced by iCAFs as Il1, considering that the inhibition of autotaxin is sufficient to inhibit NFκB in tumor cells both in *in vitro* coculture and *in vivo* models with high rates of iCAFs. The *in vitro* efficacy of the

combinatorial treatment translates into a marked synergism in an immunocompetent orthotopic PDAC model. Indeed, the combination of IOA-289 and galunisertib yields a synergistic effect in increasing the sensitivity of PDAC tumors to chemotherapy, despite the limited effect of single agents. Our data also demonstrate that combined inhibition of autotaxin and TGFβ signaling is well tolerated in mice and does not cause apparent side effects.

To the best of our knowledge, this is the first study evaluating *in vivo* the combination of a TGFβ inhibitor with IOA-289, the most advanced among the autotaxin inhibitors patented to date in clinical development (37). IOA-289 is a highly potent and selective autotaxin inhibitor developed by iOnctura for the treatment of highly fibrotic solid tumors. On a healthy volunteer study (NCT05027568), IOA-289 administered in single ascending oral doses showed good safety profile and was well tolerated. Dose-dependent increases of plasma IOA-289 were observed, corresponding with a decrease in levels of circulating LPA species measured by LC/MS (38). IOA-289 is the only autotaxin inhibitor developed for oncology indications compared with other autotaxin inhibitors that were investigated in patients with fibrotic disease (39). In a phase Ib, open-label, dose-escalation study we are currently evaluating the safety and tolerability of escalating doses of IOA-289 in patients with metastatic PDAC in combination with standard chemotherapy consisting of gemcitabine and nab-paclitaxel. Blood and tumor samples for pharmacokinetic and pharmacodynamic analyses are collected and assessments for determination of any clinical efficacy will be completed (ClinicalTrials.gov Identifier: NCT05586516).

However, this study does have certain limitations. While we were able to ascertain that Cxcl1 is the cytokine most significantly modulated *in vivo* by the inhibition of the autotaxin/LPA/NFκB axis, and that this modulation significantly reduced the infiltration of granulocytic MDSCs while enhancing the recruitment of $CD8^+$ tumor-infiltrating T cells, we cannot definitively assert that the antitumor effect of autotaxin inhibition is directly linked to this immune response. The primary mechanism proposed for the antitumor effect of autotaxin inhibition in combination with galunisertib and chemotherapy still centers on the inhibition of the antiapoptotic transcription factor NFκB in tumor cells. Whether the augmented infiltration of $CD8^+$ T lymphocytes into tumors due to autotaxin inhibition could serve as another causal mechanism for an antitumor immune response requires further investigation through studies involving combinations with immune checkpoint inhibitors and T-cell depletion experiments. Moreover, a different TGFβ targeting agent recently demonstated efficacy in combination with standard chemotherapeutic agents by reducing the immunosuppressive microenvironment in poorly immunogenic PDAC models. This effect was independent from T cells activity (40). TGFβ is, indeed, recognized as a pivotal driver of immune evasion and a critical barrier to the effectiveness of immune checkpoint inhibitors. Consequently, combined therapeutic strategies involving TGFβ and PD-1/PD-L1 inhibition have been explored in various clinical trials. However, the incorporation of TGFβ inhibitors has often failed to add a meaningful benefit to the current PD-1 or PD-L1 inhibitors (41). We recently investigated the combination of galunisertib and the anti-PD-L1 antibody durvalumab in a phase Ib study involving 32 patients with metastatic PDAC that had progressed on ≤2 prior systemic regimens. While this approach was generally well tolerated, we observed only limited clinical activity in this setting (15). In this context, the combined treatment approach of galunisertib plus IOA-289 might offer promise for further investigation in conjunction with immune checkpoint inhibitors for this disease.

In conclusion, this study demonstrates autotaxin as a novel mechanism of adaptive response to the inhibition of TGFβ. Within the PDAC microenvironment, autotaxin secreted by iCAF in response to galunisertib sustains the activation of a LPA-NFκB-Cxcl1 axis in tumor cells, and in turn, resistance to chemotherapy. The role of autotaxin in patients enrolled in the randomized phase II H9H-MC-JBAJ study further supports this model. Importantly, our study provides the preclinical rationale for investigating the autotaxin inhibitor IOA-289 plus inhibitors of TGFβ pathway in combination with classic chemotherapy in patients affected by this aggressive disease.

Authors' Disclosures

G. Di Conza is an employee at iOnctura SA. M. Lahn reports other support from iOnctura during the conduct of the study and other support from iOnctura outside the submitted work; in addition, M.M. Lahn has a patent for Use of an autotoxin Inhibitor in combination with an ALK5 inhibitors pending. D. Melisi reports grants and personal fees from iOnctura SA and grants from Associazione Italiana per la Ricerca sul Cancro (AIRC), Italian Ministry of Health, and Italian Ministry of University and Research during the conduct of the study; in addition, D. Melisi reports personal fees from iOnctura outside the submitted work. No disclosures were reported by the other authors.

Authors' Contributions

S. Pietrobono: Conceptualization, data curation, formal analysis, supervision, validation, investigation, methodology, writing–original draft, writing–review and editing. **F. Sabbadini:** Data curation, formal analysis, validation, investigation, methodology. **M. Bertolini:** Validation, investigation. **D. Mangiameli:** Validation, investigation. **V. De Vita:** Validation, investigation. **F. Fazzini:** Investigation. **G. Lunardi:** Validation. **S. Casalino:** Validation, investigation. **E. Scarlato:** Investigation. **V. Merz:** Validation, investigation. **C. Zecchetto:** Validation, investigation. **A. Quinzii:** Validation, investigation. **G. Di Conza:** Resources, supervision, funding acquisition, writing–review and editing. **M. Lahn:** Resources, supervision, funding acquisition, writing–review and editing. **D. Melisi:** Conceptualization, resources, supervision, funding acquisition, writing–original draft, writing–review and editing.

Acknowledgments

This study was supported by Associazione Italiana per la Ricerca sul Cancro (AIRC) grant 23719 (D. Melisi), Italian Ministry of Health grant GR-2016-02361134 (D. Melisi), Italian Ministry of University and Research under PNRR -M4C2- I1.3 Project PE_00000019 "HEAL ITALIA" (D. Melisi), Associations "Nastro Viola" and "Voglio il Massimo" (D. Melisi). This study was also supported by an unrestricted grant by iOnctura SA. Part of the work was performed at the Laboratorio Universitario di Ricerca Medica (LURM) Research Center, University of Verona. We thank Dr. Hayley Louise Salt for data entry and administrative support.

The publication costs of this article were defrayed in part by the payment of publication fees. Therefore, and solely to indicate this fact, this article is hereby marked "advertisement" in accordance with 18 USC section 1734.

Note

Supplementary data for this article are available at Cancer Research Online (http://cancerres.aacrjournals.org/).

Received January 10, 2023; revised August 11, 2023; accepted September 20, 2023; published first September 22, 2023.

References

1. Halbrook CJ, Lyssiotis CA, Pasca di Magliano M, Maitra A. Pancreatic cancer: advances and challenges. Cell 2023;186:1729–54.
2. Siegel RL, Miller KD, Wagle NS, Jemal A. Cancer statistics, 2023. CA Cancer J Clin 2023;73:17–48.

3. Rahib L, Wehner MR, Matrisian LM, Nead KT. Estimated projection of US cancer incidence and death to 2040. JAMA Netw Open 2021;4:e214708.
4. Tamburrino A, Piro G, Carbone C, Tortora G, Melisi D. Mechanisms of resistance to chemotherapeutic and anti-angiogenic drugs as novel targets for pancreatic cancer therapy. Front Pharmacol 2013;4:56.
5. Bailey P, Chang DK, Nones K, Johns AL, Patch AM, Gingras MC, et al. Genomic analyses identify molecular subtypes of pancreatic cancer. Nature 2016;531:47–52.
6. Sabbadini F, Bertolini M, De Matteis S, Mangiameli D, Contarelli S, Pietrobono S, et al. The multifaceted role of TGF-beta in gastrointestinal tumors. Cancers 2021; 13:3960.
7. Santoro R, Zanotto M, Simionato F, Zecchetto C, Merz V, Cavallini C, et al. Modulating TAK1 expression inhibits YAP and TAZ oncogenic functions in pancreatic cancer. Mol Cancer Ther 2020;19:247–57.
8. Biffi G, Tuveson DA. Diversity and biology of cancer-associated fibroblasts. Physiol Rev 2021;101:147–76.
9. Biffi G, Oni TE, Spielman B, Hao Y, Elyada E, Park Y, et al. IL1-induced JAK/STAT signaling is antagonized by TGFbeta to shape CAF heterogeneity in pancreatic ductal adenocarcinoma. Cancer Discov 2019;9:282–301.
10. Melisi D, Xia Q, Paradiso G, Ling J, Moccia T, Carbone C, et al. Modulation of pancreatic cancer chemoresistance by inhibition of TAK1. J Natl Cancer Inst 2011;103:1190–204.
11. Melisi D, Ishiyama S, Sclabas GM, Fleming JB, Xia Q, Tortora G, et al. LY2109761, a novel transforming growth factor beta receptor type I and type II dual inhibitor, as a therapeutic approach to suppressing pancreatic cancer metastasis. Mol Cancer Ther 2008;7:829–40.
12. Melisi D, Garcia-Carbonero R, Macarulla T, Pezet D, Deplanque G, Fuchs M, et al. Galunisertib plus gemcitabine vs. gemcitabine for first-line treatment of patients with unresectable pancreatic cancer. Br J Cancer 2018;119: 1208–14.
13. Melisi D, Garcia-Carbonero R, Macarulla T, Pezet D, Deplanque G, Fuchs M, et al. TGFbeta receptor inhibitor galunisertib is linked to inflammation- and remodeling-related proteins in patients with pancreatic cancer. Cancer Chemother Pharmacol 2019;83:975–91.
14. Gueorguieva I, Tabernero J, Melisi D, Macarulla T, Merz V, Waterhouse TH, et al. Population pharmacokinetics and exposure-overall survival analysis of the transforming growth factor-beta inhibitor galunisertib in patients with pancreatic cancer. Cancer Chemother Pharmacol 2019;84:1003–15.
15. Melisi D, Oh DY, Hollebecque A, Calvo E, Varghese A, Borazanci E, et al. Safety and activity of the TGFbeta receptor I kinase inhibitor galunisertib plus the anti-PD-L1 antibody durvalumab in metastatic pancreatic cancer. J Immunother Cancer 2021;9:e002068.
16. Yap TA, Vieito M, Baldini C, Sepulveda-Sanchez JM, Kondo S, Simonelli M, et al. First-in-human phase I study of a next-generation, oral, TGFbeta receptor 1 inhibitor, LY3200882, in patients with advanced cancer. Clin Cancer Res 2021; 27:6666–76.
17. Tokumura A, Majima E, Kariya Y, Tominaga K, Kogure K, Yasuda K, et al. Identification of human plasma lysophospholipase D, a lysophosphatidic acid-producing enzyme, as autotaxin, a multifunctional phosphodiesterase. J Biol Chem 2002;277:39436–42.
18. Benesch MG, Ko YM, McMullen TP, Brindley DN. Autotaxin in the crosshairs: taking aim at cancer and other inflammatory conditions. FEBS Lett 2014;588: 2712–27.
19. Tang X, Benesch MGK, Brindley DN. Role of the autotaxin-lysophosphatidate axis in the development of resistance to cancer therapy. Biochim Biophys Acta Mol Cell Biol Lipids 2020;1865:158716.
20. Ohlund D, Handly-Santana A, Biffi G, Elyada E, Almeida AS, Ponz-Sarvise M, et al. Distinct populations of inflammatory fibroblasts and myofibroblasts in pancreatic cancer. J Exp Med 2017;214:579–96.
21. Melisi D, Ossovskaya V, Zhu C, Rosa R, Ling J, Dougherty PM, et al. Oral poly (ADP-ribose) polymerase-1 inhibitor BSI-401 has antitumor activity and synergizes with oxaliplatin against pancreatic cancer, preventing acute neurotoxicity. Clin Cancer Res 2009;15:6367–77.
22. Ullman-Cullere MH, Foltz CJ. Body condition scoring: a rapid and accurate method for assessing health status in mice. Lab Anim Sci 1999;49:319–23.
23. Deken MA, Niewola-Staszkowska K, Peyruchaud O, Mikulcic N, Antolic M, Shah P, et al. Characterization and translational development of IOA-289, a novel autotaxin inhibitor for the treatment of solid tumors. Immunooncol Technol 2023;18:100384.
24. Matas-Rico E, Frijlink E, van der Haar Avila I, Menegakis A, van Zon M, Morris AJ, et al. Autotaxin impedes anti-tumor immunity by suppressing chemotaxis and tumor infiltration of CD8(+) T cells. Cell Rep 2021;37: 110013.
25. Aiello S, Casiraghi F. Lysophosphatidic acid: promoter of cancer progression and of tumor microenvironment development. a promising target for anticancer therapies? Cells 2021;10:1390.
26. Mazzocca A, Dituri F, Lupo L, Quaranta M, Antonaci S, Giannelli G. Tumor-secreted lysophostatidic acid accelerates hepatocellular carcinoma progression by promoting differentiation of peritumoral fibroblasts in myofibroblasts. Hepatology 2011;54:920–30.
27. Melisi D, Chiao PJ. NF-kappa B as a target for cancer therapy. Expert Opin Ther Targets 2007;11:133–44.
28. Devalaraja MN, Wang DZ, Ballard DW, Richmond A. Elevated constitutive IkappaB kinase activity and IkappaB-alpha phosphorylation in Hs294T melanoma cells lead to increased basal MGSA/GRO-alpha transcription. Cancer Res 1999;59:1372–7.
29. Wan F, Lenardo MJ. Specification of DNA binding activity of NF-kappaB proteins. Cold Spring Harb Perspect Biol 2009;1:a000067.
30. Korbecki J, Barczak K, Gutowska I, Chlubek D, Baranowska-Bosiacka I. CXCL1: gene, promoter, regulation of expression, mRNA stability, regulation of activity in the intercellular space. Int J Mol Sci 2022;23:792.
31. Acharyya S, Oskarsson T, Vanharanta S, Malladi S, Kim J, Morris PG, et al. A CXCL1 paracrine network links cancer chemoresistance and metastasis. Cell 2012;150:165–78.
32. Li J, Byrne KT, Yan F, Yamazoe T, Chen Z, Baslan T, et al. Tumor cell-intrinsic factors underlie heterogeneity of immune cell infiltration and response to immunotherapy. Immunity 2018;49:178–93.
33. Veglia F, Sanseviero E, Gabrilovich DI. Myeloid-derived suppressor cells in the era of increasing myeloid cell diversity. Nat Rev Immunol 2021;21: 485–98.
34. Auciello FR, Bulusu V, Oon C, Tait-Mulder J, Berry M, Bhattacharyya S, et al. A stromal lysolipid-autotaxin signaling axis promotes pancreatic tumor progression. Cancer Discov 2019;9:617–27.
35. Yung YC, Stoddard NC, Chun J. LPA receptor signaling: pharmacology, physiology, and pathophysiology. J Lipid Res 2014;55:1192–214.
36. Carbone C, Melisi D. NF-kappaB as a target for pancreatic cancer therapy. Expert Opin Ther Targets 2012;16 Suppl 2:S1–10.
37. Bano S, Al-Rashida M, Alharthy RD, Khan IA, Iqbal J. Nucleotide pyrophosphatase/phosphodiesterases (NPPs) including NPP1 and NPP2/ATX as important drug targets: a patent review (2015–2020). Expert Opin Ther Pat 2022;32: 743–51.
38. Johnson Z, Deken M, Medhi R, Maggs L, Carruthers A, Cheasty A, et al. Targeting autotaxin to suppress stromal signaling in the tumor microenvironment to improve outcome to therapy in fibrotic tumor types [abstract]. In: Proceedings of the American Association for Cancer Research Annual Meeting 2022; 2022 Apr 8–13. Philadelphia (PA): AACR; Cancer Res 2022;82(12_Suppl): Abstract nr 2636.
39. Jia Y, Li Y, Xu XD, Tian Y, Shang H. Design and development of autotaxin inhibitors. Pharmaceuticals 2021;14:1203.
40. Qiang L, Hoffman MT, Ali LR, Castillo JI, Kageler L, Temesgen A, et al. Transforming growth factor-beta blockade in pancreatic cancer enhances sensitivity to combination chemotherapy. Gastroenterology 2023;165:874–90.
41. Gulley JL, Schlom J, Barcellos-Hoff MH, Wang XJ, Seoane J, Audhuy F, et al. Dual inhibition of TGF-beta and PD-L1: a novel approach to cancer treatment. Mol Oncol 2022;16:2117–34.